engineering proceedings

MDPI

Proceeding Paper

Performance Assessment of Aerogel-Based Transparent Insulation in Building-Integrated Natural Convection Solar Air Collectors †

Yusuf Kepir [1,*], Holger Seidlitz [1,2], Lars Ulke-Winter [1] and Felix Kuke [1,2]

[1] Faculty 3 Mechanical Engineering, Electrical and Energy Systems, Brandenburg University of Technology Cottbus–Senftenberg (BTU), 03046 Cottbus, Germany; holger.seidlitz@b-tu.de (H.S.); lars.ulke-winter@b-tu.de (L.U.-W.); felix.kuke@iap.fraunhofer.de (F.K.)
[2] Research Division Polymeric Materials and Composites PYCO, Fraunhofer Institute for Applied Polymer Research IAP, 15745 Wildau, Germany
* Correspondence: yusuf.kepir@b-tu.de
† Presented at the 3rd International Online Conference on Energies (IOCEN 2026), 12–15 May 2026. Available online: https://sciforum.net/event/IOCEN2026.

Abstract

This study presents a comparative numerical assessment of three transparent cover configurations for a building-integrated natural convection solar air collector: low-iron tempered glass, an aerogel-filled polycarbonate panel, and monolithic silica aerogel. A three-dimensional steady-state CFD model was developed using ANSYS Fluent under identical solar and ambient boundary conditions. Compared with low-iron glass, monolithic aerogel increased the outlet air temperature from 326.4 K to 360.1 K, useful heat gain from 647.25 W to 1629.91 W, and thermal efficiency from 32.3% to 81.5%, indicating improved thermal performance under the investigated numerical conditions. A five-level mesh refinement study supported the selection of the 285,380-element mesh based on the stability of outlet temperature and mass flow rate. These findings indicate the potential of monolithic aerogel for passive solar air heating under the investigated conditions.

Keywords: aerogel; solar air collectors; CFD analysis; transparent insulation materials; natural convection

1. Introduction

The building and construction sector contributes substantially to global energy demand and emissions, accounting for approximately 32% of global energy consumption and 34% of global CO_2 emissions [1]. Therefore, building-integrated renewable thermal systems are important for reducing operational energy use. Solar air collectors are simple and low-maintenance systems for converting incident solar radiation into useful heat for space heating, ventilation-air preheating, drying, and façade-integrated applications [2].

The performance of a solar air collector depends on maximizing absorbed solar radiation while minimizing cover-related heat losses. Conventional glass provides high solar transmittance but limited thermal insulation, particularly under cold ambient conditions or elevated absorber temperatures. Transparent insulation materials, including polymer sheets, honeycomb/capillary structures, vacuum glazing, granular aerogel systems, and monolithic aerogel configurations, have therefore been investigated to reduce heat losses while preserving solar transmission [3,4].

Check for updates

Academic Editor: Piero Bevilacqua

Published: 30 September 2026

Copyright: © 2026 by the authors. Licensee MDPI, Basel, Switzerland. This article is an open access article distributed under the terms and conditions of the Creative Commons Attribution (CC BY) license.

Silica aerogels are attractive for this purpose because of their low thermal conductivity, low density, high porosity, and optical transparency. Aerogel-based building-envelope and glazing systems have shown potential for thermal superinsulation and improved glazing performance [5–7]. In solar thermal applications, Zhao et al. demonstrated that optimized transparent monolithic silica aerogels can enable temperatures above 265 °C under unconcentrated sunlight [8].

However, monolithic aerogels remain challenging in terms of brittleness, scalability, production cost, and long-term durability. Rapid supercritical extraction methods may help reduce production time and support scalable fabrication [9,10], but the collector-level benefit of monolithic aerogel glazing still requires quantitative assessment.

The present study provides a comparative numerical assessment of low-iron glass, aerogel-filled multiwall polycarbonate, and monolithic silica aerogel covers in a natural convection solar air collector under identical boundary conditions, focusing on outlet air temperature, absorber temperature, mass flow rate, useful heat gain, and thermal efficiency. The novelty of this work lies in quantifying the thermodynamic synergy between high solar transmittance and passive buoyancy-driven flow acceleration, establishing numerical grid independence across five mesh resolutions, and evaluating system sensitivity under variable irradiance conditions.

2. Materials and Methods

2.1. Solar Air Collector Configuration

A 1 × 2 m flat-plate solar air collector was modeled as a building-integrated natural convection system. The absorber was defined as Tinox-coated aluminum with a solar absorptivity of 0.95 and a thermal emissivity of 0.05.

The collector was subjected to an incident solar radiation intensity of 1000 W/m^2, resulting in a total incident solar input of 2000 W over the 2 m^2 absorber area. The solar collector model is shown in Figure 1.

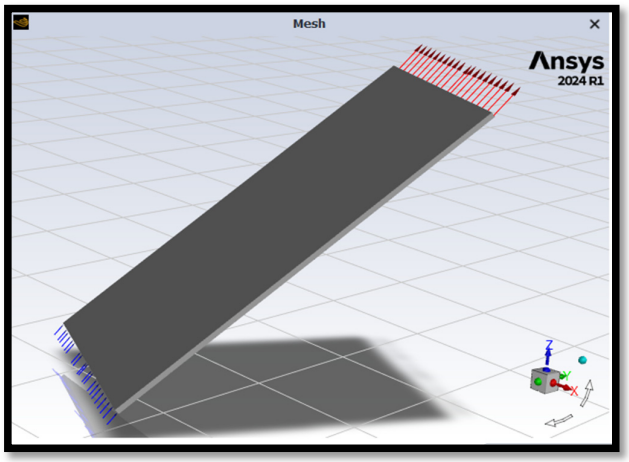

Figure 1. The solar collector model with inlet and outlet flow boundary indications.

2.2. Glazing Configurations

Three transparent cover configurations were investigated: 4 mm low-iron tempered glass, a 20 mm aerogel-particle-filled multiwall polycarbonate panel, and a 20 mm monolithic silica aerogel layer.

U-values and solar transmittances listed in Table 1 represent effective macroscopic properties and were not directly entered as uniform boundary conditions in the CFD solver. Instead, glazing covers were modeled as physical solid zones with their respective thicknesses (4 mm for glass, 20 mm for aerogels), thermal conductivities

(k = 1.15 W/mK for glass, 0.025 W/mK for granular PC, and 0.018 W/mK for monolithic aerogel), and spectral optical absorption/scattering properties inside the Discrete Ordinates (DO) radiation model.

Table 1. Effective thermal and optical parameters of the investigated glazing configurations.

Configuration	Thickness	U-Value	Solar Transmittance
Low-iron tempered glass	4 mm	5.8 W/m^{2}K	0.90
Aerogel-filled multiwall polycarbonate panel	20 mm	0.98 W/m^{2}K	0.52
Monolithic silica aerogel	20 mm	0.54 W/m^{2}K	0.85

The low-iron tempered glass served as the reference case. The aerogel-filled polycarbonate panel represents a practical and mechanically robust transparent insulation option, while monolithic silica aerogel represents the high-performance case due to its combination of low U-value and high solar transmittance. Similar trade-offs have been reported for transparent insulation and aerogel glazing systems [3,4,6,7].

2.3. Numerical Model

The numerical simulations were carried out using ANSYS Fluent 2024 R1 (ANSYS, Inc., Canonsburg, PA, USA). A three-dimensional steady-state CFD model was developed to evaluate natural convection, conduction through the cover, absorber-to-air convective heat transfer, and radiative solar energy input.

Governing equations for mass, momentum, and energy were solved using the pressure-based Coupled solver with a pseudo-transient formulation to accelerate steady-state convergence. Spatial discretization of pressure employed the Second-Order scheme, while momentum, energy, turbulence kinetic energy, and specific dissipation rate equations utilized the Second-Order Upwind scheme.

Air density was modeled using the incompressible ideal gas formulation to capture buoyancy-driven flow. The k–ω SST turbulence model was selected for its near-wall performance and robustness in engineering applications [11].

Radiative heat transfer was resolved using the non-gray Discrete Ordinates radiation model, which was divided into two distinct spectral bands. The first spectral band spanned from 0 to 2.5 µm to account for short-wave solar radiation with a spectral fraction of 0.95, whereas the second spectral band covered wavelengths from 2.5 to 100 µm to model long-wave thermal radiation [12]. For the semi-transparent monolithic aerogel cover, the refractive index was defined as 1.05. Furthermore, the spectral absorption coefficient in the first band was set to 0.1 m^{-1} to facilitate high solar energy transmission, while the absorption coefficient in the second band was assigned a value of 300 m^{-1} to effectively block long-wave thermal back-radiation and replicate the greenhouse effect. Convergence criteria were strictly enforced across all governing equations, requiring residual target limits of 10^{-8} for energy, 10^{-6} for Discrete Ordinates radiation intensity, and 10^{-4} for continuity, velocity, turbulence kinetic energy, and specific dissipation rate residuals.

2.4. Mesh Generation and Numerical Consistency

The computational domain was discretized using ANSYS Meshing with local structured refinement within the air channel and dedicated prism inflation layers along the solid boundaries to capture boundary layer effects. To establish the grid independence of the numerical solution, a systematic study was conducted across five distinct grid resolutions ranging from 69,965 to 6,796,900 elements (DP1 to DP5), ensuring proper resolution of

the viscous sublayer for the k–ω SST turbulence model. As shown in Table 2, refining the grid from 285,380 elements (DP3) to 908,190 elements (DP4) produced a variation of only 0.125% in predicted outlet air temperature (Tout = 360.20 K) and 0.124% in mass flow rate (0.024205 kg/s). Further mesh refinement to 6,796,900 elements (DP5) resulted in a negligible temperature change of 0.055% and mass flow change of 0.108% (0.024179 kg/s).

Table 2. Grid independence study results across five mesh resolutions (DP1–DP5) under 1000 W/m^2 irradiance.

Design Point	Element Size	Elements	Tout (K)	Tabs (K)	Mass Flow Rate (kg/s)	ΔTout Variation (%)	Δmdot Variation (%)
DP1	10 mm	69,965	358.98	383.38	0.029796	N/A	N/A
DP2	8 mm	133,340	359.31	382.82	0.025382	0.092%	14.81%
DP3	6 mm	285,380	359.75	381.20	0.024235	0.122%	4.53%
DP4	4 mm	908,190	360.20	380.95	0.024205	0.125%	0.124%
DP5	2 mm	6,796,900	360.40	381.04	0.024179	0.055%	0.108%

Consequently, the DP3 mesh (285,380 elements) was selected for all simulations to strike an optimal balance between numerical accuracy and computational efficiency. Figure 2 illustrates the computational mesh structure of the solar air collector model, featuring local grid refinement within the fluid channel and fine prism inflation layers along the solid boundaries to adequately resolve boundary layer effects.

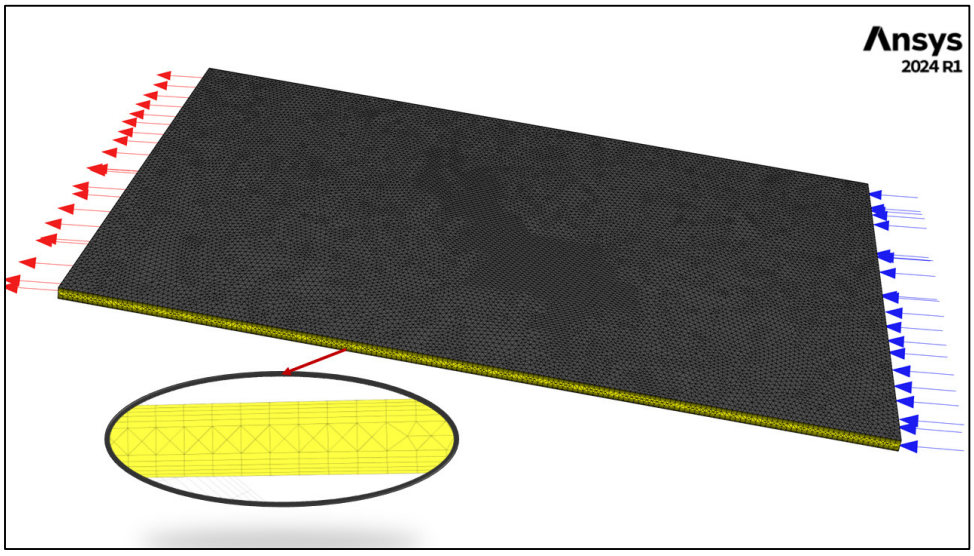

Figure 2. Computational mesh of the solar air collector model with a magnified view of the representative boundary mesh structure used along the inlet, outlet, and side walls.

2.5. Boundary Conditions

The solar analyses were performed based on the coordinates of the city of Cottbus, located in the state of Brandenburg, Germany. In the Solar Calculator module, the longitude was set to 14.33, the latitude to 51.77, and the time to 13:00 on 21 June. The same boundary conditions were applied to all glazing configurations to ensure a direct comparison. The inlet air temperature was set to 293.15 K, corresponding to 20 °C. The inlet and outlet were both defined using pressure boundary conditions of 0 Pa gauge pressure, allowing buoyancy-driven flow development under the imposed thermal field. The incident solar radiation intensity was set to 1000 W/m^2. Environmental heat exchange at the outer cover was represented by a mixed convective boundary condition with a free-stream temperature

of 293.15 K and an external convective heat transfer coefficient of 10 W/m^{2}K. Table 3 lists the boundary conditions applied in Fluent.

Table 3. Boundary conditions used in the CFD simulations.

Parameter	Value
Inlet temperature	293.15 K
Inlet type	Pressure inlet
Inlet pressure	0 Pa gauge
Outlet pressure	0 Pa gauge
Ambient temperature	293.15 K
Solar radiation intensity	1000 W/m^2
Absorber area	2 m^2
External heat transfer coefficient	10 W/m^{2}K

2.6. Performance Calculations

The useful heat gain of the solar air collector was calculated using the standard energy balance expression for solar thermal collectors [13]:

$$Q_u = m_{dot}\, c_p\, (T_{out} - T_{in}) \quad (1)$$

where Q_u is the useful heat gain, m_{dot} is the air mass flow rate, c_p is the specific heat capacity of air, T_{out} is the outlet air temperature, and T_{in} is the inlet air temperature.

The incident solar power was calculated as:

$$Q_s = I_s\, A \quad (2)$$

where I_s is the solar radiation intensity and A is the absorber area. The thermal efficiency was then obtained as:

$$\eta = Q_u / Q_s \quad (3)$$

For all cases, c_p was taken as 1006 J/kg·K, I_s was 1000 W/m^2, and A was 2 m^2.

3. Results and Discussion

3.1. Thermal, Flow and Efficiency Performance

The numerical results indicated that replacing conventional low-iron glass with aerogel-based transparent insulation improved outlet air temperature, absorber temperature, mass flow rate, useful heat gain, and thermal efficiency. The results are presented in Figure 3 and Table 4. Under identical boundary conditions, the monolithic aerogel configuration provided the highest comparative performance.

Table 4. Comparative numerical results for the investigated glazing configurations.

Glazing Material	T_{out} (K)	T_{abs} (K)	m_{dot} (kg/s)	Q_u (W)	η (%)
Low-iron tempered glass	326.4	350.9	0.01935	647.25	32.3
Aerogel-filled PC panel	345.3	363.9	0.02220	1164.68	58.2
Monolithic aerogel	360.1	381.8	0.02420	1629.91	81.5

Compared with the glass-covered collector, the monolithic aerogel increased outlet air temperature from 326.4 K to 360.1 K and absorber temperature from 350.9 K to 381.8 K. The mass flow rate increased from 0.01935 kg/s to 0.02420 kg/s, while useful heat gain increased from 647.25 W to 1629.91 W. Consequently, the calculated thermal efficiency increased from 32.3% to 81.5%.

https://doi.org/10.3390/engproc2026147021

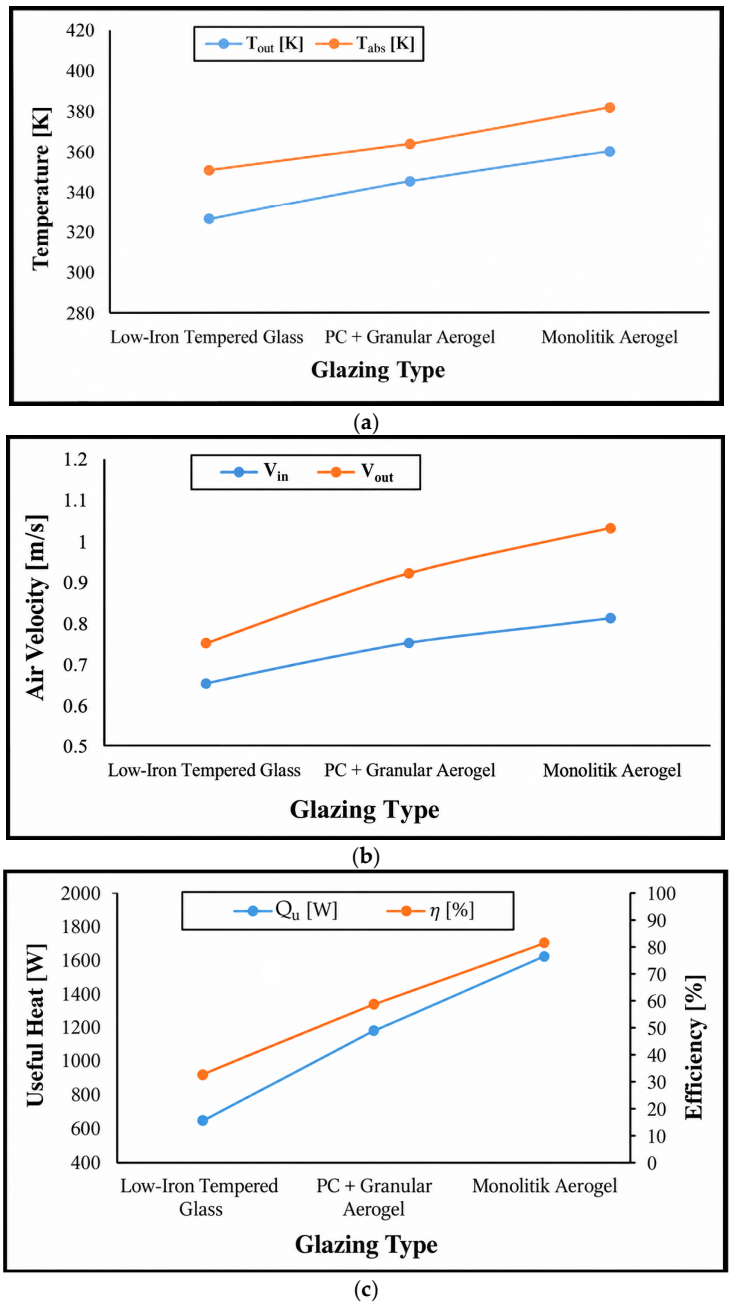

Figure 3. Comparison of the numerical results for all glazing configurations: (**a**) outlet and absorber temperatures; (**b**) inlet and outlet velocities; (**c**) useful heat gain and thermal efficiency.

The baseline thermal efficiency of 32.3% obtained for the low-iron glass collector falls comfortably within the standard benchmark range of 30% to 45% reported for passive solar air collectors. Furthermore, the high thermal performance of the monolithic aerogel configuration, reaching an efficiency of 81.5% and an absorber temperature of 381.8 K (108.65 °C), aligns closely with the experimental findings of Zhao et al., who demonstrated that transparent monolithic silica aerogels function as highly efficient 'thermal traps' that minimize both convective and radiative heat losses to enable unconcentrated solar receivers to operate at temperatures exceeding 200 °C.

The top-view temperature contours obtained from the CFD simulations are presented in Figure 4. The contours illustrate the temperature development along the collector for each glazing configuration and provide a visual comparison of the thermal response under identical boundary conditions.

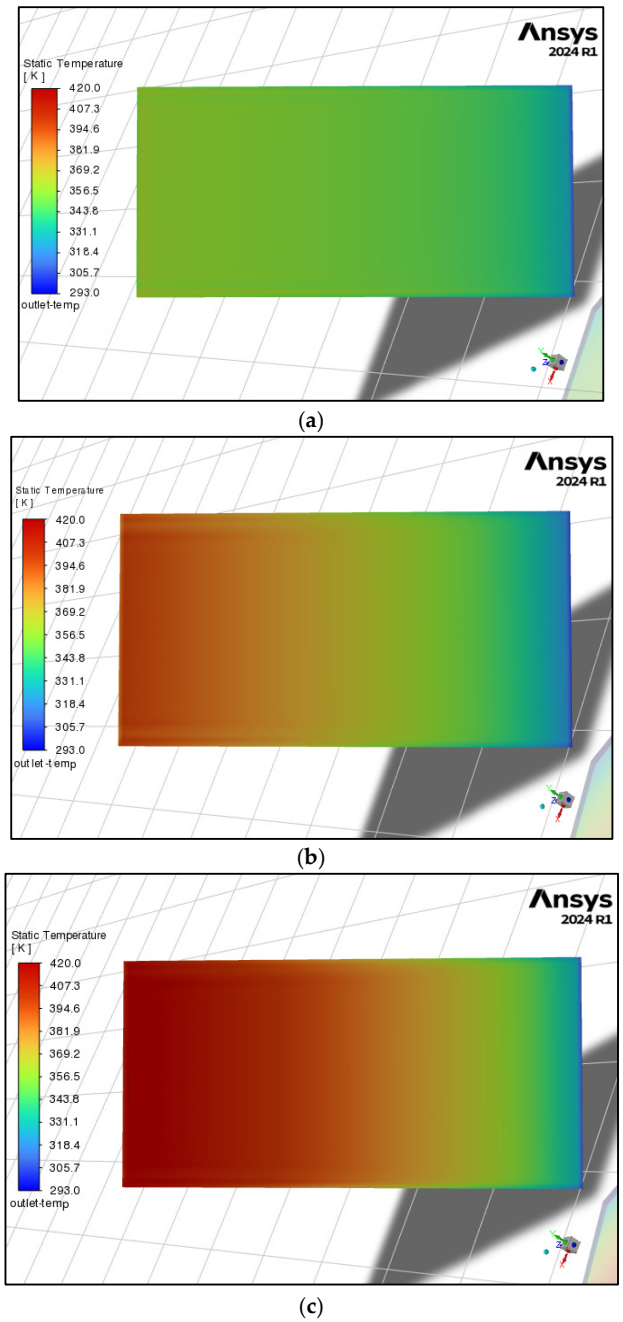

Figure 4. Top-view temperature contour distributions of the solar air collector for the investigated glazing configurations: (**a**) low-iron tempered glass; (**b**) aerogel-particle-filled multiwall polycarbonate panel; (**c**) monolithic silica aerogel. The red arrows indicate the airflow direction.

The aerogel-filled polycarbonate panel showed intermediate performance, with an outlet temperature of 345.3 K, useful heat gain of 1164.68 W, and thermal efficiency of 58.2%. This confirms that reduced cover heat losses improve performance, but the lower solar transmittance of granular aerogel-filled panels limits the energy reaching the absorber.

The performance differences among the glazing configurations are mainly related to the combined influence of thermal insulation and solar transmittance. While the aerogel-filled polycarbonate panel improved the collector performance compared with low-iron glass, its lower solar transmittance limited the thermal output relative to the monolithic aerogel case. The monolithic aerogel configuration provided the most favorable balance between effective solar transmission and cover-related heat-loss reduction under the investigated numerical conditions.

https://doi.org/10.3390/engproc2026147021

3.2. Thermosyphon Flow Mechanics and Velocity Acceleration

The physical mechanism driving fluid flow through the collector is the thermosyphon effect, governed by buoyancy forces. As the absorber plate absorbs solar irradiance, it heats the adjacent air boundary layer, reducing its density according to the incompressible ideal gas law. This density gradient creates a gravitational pressure differential between the cold inlet and hot outlet, acting as a passive thermodynamic driving force. Under identical solar boundary conditions, the ultra-low thermal conductivity of the monolithic aerogel (k = 0.018 W/mK) suppresses top heat losses from the front cover, maintaining a significantly elevated absorber temperature (381.8 K). This elevated thermal field strengthens the buoyancy force, passively accelerating the air flow from 0.65 m/s (glass reference) to 0.81 m/s, yielding a 25% increase in buoyancy-driven mass flow rate (from 0.01935 kg/s to 0.024205 kg/s) without auxiliary fan consumption. As illustrated in Figure 5, the elevated thermal field generated by the monolithic aerogel cover passively accelerates the buoyancy-driven airflow along the vertical collector domain from the inlet to the outlet.

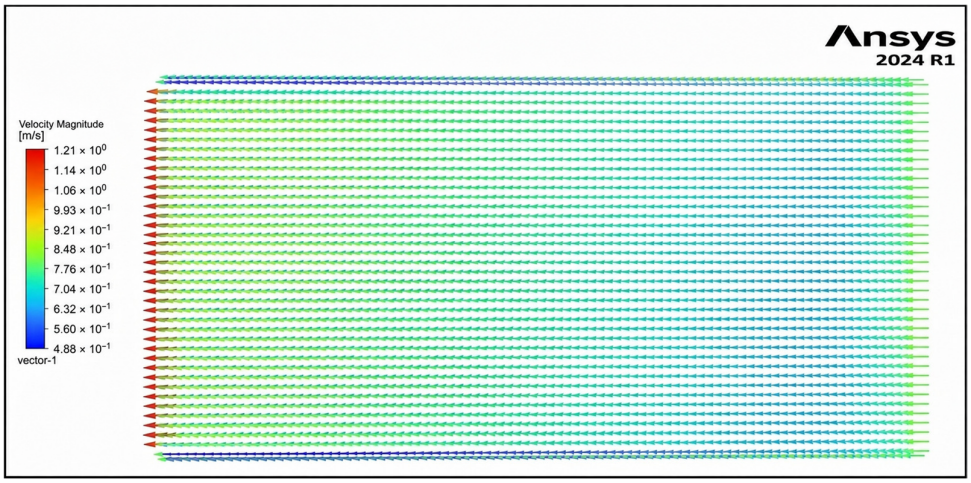

Figure 5. Velocity vector distribution along the entire domain of the monolithic aerogel solar air collector, illustrating buoyancy-driven natural convection flow acceleration from the inlet to the outlet.

3.3. Sensitivity Analysis Under Variable Solar Irradiance

To evaluate the operational robustness of the monolithic aerogel system under variable climatic conditions, a sensitivity analysis was performed for solar irradiance levels of 1000, 800, and 600 W/m^2.

As demonstrated in Table 5, even when solar irradiance drops to 600 W/m^2 under overcast or cold winter conditions, the monolithic aerogel collector maintains an outlet temperature of 337.9 K (64.75 °C), corresponding to a temperature rise of 44.75 K above ambient (293.15 K). These results confirm that the monolithic aerogel cover retains exceptional thermal insulation and delivers useful heat gain even under sub-optimal solar radiation.

Table 5. Thermal response of the monolithic aerogel collector under variable solar irradiance levels.

Solar Irradiance (Is)	Tabs (K/°C)	Tout (K/°C)	ΔT Rise Above Ambient (K)
1000 W/m^2	381.8 K (108.65 °C)	360.1 K (86.95 °C)	66.95 K
800 W/m^2	367.2 K (94.05 °C)	349.7 K (76.55 °C)	56.55 K
600 W/m^2	349.4 K (76.25 °C)	337.9 K (64.75 °C)	44.75 K

3.4. Collector Footprint and Life-Cycle Considerations

While monolithic silica aerogel currently incurs higher material costs than standard tempered glass, its superior insulation reduces the required collector footprint by up to 43% (from 5.73 m^2 for granular aerogel baseline to 3.28 m^2 for monolithic aerogel, and down to 2.98 m^2) to meet an equivalent space heating load under cold winter conditions (Cottbus, IT = 600 W/m^2). This ~43% reduction in required surface area directly offsets higher raw material costs by lowering structural frame requirements, installation labor, and building facade footprint. Furthermore, from a life-cycle perspective, recent advancements in Rapid Supercritical Extraction (RSCE) fabrication techniques by Carroll et al. [9] and Bhuiya et al. [10] significantly reduce manufacturing cycle times and embodied energy, enhancing the overall sustainability and payback period of building-integrated monolithic aerogel systems.

4. Conclusions

This study presented a comparative numerical assessment of three transparent cover configurations for a building-integrated natural convection solar air collector, namely low-iron tempered glass, an aerogel-filled multiwall polycarbonate panel, and monolithic silica aerogel. Under identical geometrical, solar, and boundary conditions, the monolithic aerogel configuration provided the highest thermal performance among the investigated cases.

Compared with the low-iron glass reference, the monolithic aerogel cover increased the outlet air temperature from 326.4 K to 360.1 K and the absorber temperature from 350.9 K to 381.8 K. The useful heat gain increased from 647.25 W to 1629.91 W, while the calculated thermal efficiency increased from 32.3% to 81.5%. The aerogel-filled polycarbonate panel also improved the collector performance compared with conventional glass, but its lower solar transmittance limited its thermal output relative to the monolithic aerogel case.

The results indicate that the combination of low representative U-value and high effective solar transmittance is decisive for improving the comparative performance of transparent insulation layers in solar air collectors. In this respect, monolithic silica aerogel offers a favorable balance between solar transmission and thermal insulation. Overall, the findings demonstrate the potential of aerogel-based transparent insulation, particularly monolithic silica aerogel, for enhancing the thermal performance of building-integrated natural convection solar air collectors.

In addition, numerical grid independence was rigorously established across five mesh densities (DP1–DP5), confirming that a 285,380-element grid (DP3) yields converged solution fields. Sensitivity analysis further verified that under a low irradiance of 600 W/m^2, the monolithic aerogel collector maintains a useful air outlet temperature of 337.9 K (64.75 °C).

Finally, life-cycle footprint calculations demonstrate that the super-insulating cover reduces the required collector facade area by approximately 43% (from 5.73 m^2 to 3.28 m^2) to meet equivalent space heating loads, helping offset raw material costs through lower framing and installation expenses.

Author Contributions: Conceptualization, Y.K.; methodology, Y.K.; software, Y.K.; formal analysis, Y.K.; investigation, Y.K.; data curation, Y.K.; writing—original draft preparation, Y.K.; writing—review and editing, H.S., L.U.-W. and F.K.; supervision, H.S. and L.U.-W.; project administration, H.S. All authors have read and agreed to the published version of the manuscript.

Funding: This research was carried out within the framework of the SpreeTec neXt project, funded by the Federal Ministry of Research, Technology and Space (BMFTR), grant number 02P21Z000.

Institutional Review Board Statement: Not applicable.

Informed Consent Statement: Not applicable.

Data Availability Statement: The numerical data supporting the findings of this study are available from the corresponding author upon reasonable request.

Acknowledgments: During the preparation of this manuscript, generative AI tools were used for language refinement and structural editing. The authors reviewed and edited the output and take full responsibility for the content of this publication.

Conflicts of Interest: The authors declare no conflicts of interest. The funder had no role in the design of the study; in the collection, analyses, or interpretation of data; in the writing of the manuscript; or in the decision to publish the results.

References

1. United Nations Environment Programme; Global Alliance for Buildings and Construction. *Global Status Report for Buildings and Construction 2024/2025: Not Just Another Brick in the Wall*; United Nations Environment Programme: Nairobi, Kenya, 2025.
2. Kalogirou, S.A. Solar thermal collectors and applications. *Prog. Energy Combust. Sci.* **2004**, *30*, 231–295. [CrossRef]
3. Kaushika, N.D.; Sumathy, K. Solar transparent insulation materials: A review. *Renew. Sustain. Energy Rev.* **2003**, *7*, 317–351. [CrossRef]
4. Paneri, A.; Wong, I.L.; Burek, S. Transparent insulation materials: An overview on past, present and future developments. *Sol. Energy* **2019**, *184*, 59–83. [CrossRef]
5. Cuce, E.; Cuce, P.M.; Wood, C.J.; Riffat, S.B. Toward aerogel based thermal superinsulation in buildings: A comprehensive review. *Renew. Sustain. Energy Rev.* **2014**, *34*, 273–299. [CrossRef]
6. Buratti, C.; Moretti, E. Glazing systems with silica aerogel for energy savings in buildings. *Appl. Energy* **2012**, *98*, 396–403. [CrossRef]
7. Huang, Y.; Niu, J.L. Application of super-insulating translucent silica aerogel glazing system on commercial building envelope of humid subtropical climates: Impact on space cooling load. *Energy* **2015**, *83*, 316–325. [CrossRef]
8. Zhao, L.; Bhatia, B.; Yang, S.; Strobach, E.; Weinstein, L.A.; Cooper, T.A.; Chen, G.; Wang, E.N. Harnessing heat beyond 200 °C from unconcentrated sunlight with nonevacuated transparent aerogels. *ACS Nano* **2019**, *13*, 7508–7516. [CrossRef]
9. Carroll, M.K.; Anderson, A.M.; Gorka, C.A. Preparing silica aerogel monoliths via a rapid supercritical extraction method. *J. Vis. Exp.* **2014**, *84*, e51421. [CrossRef]
10. Bhuiya, M.M.H.; Anderson, A.M.; Carroll, M.K.; Bruno, B.A.; Ventrella, J.L.; Silberman, B.; Keramati, B. Preparation of monolithic silica aerogel for fenestration applications: Scaling up, reducing cycle time, and improving performance. *Ind. Eng. Chem. Res.* **2016**, *55*, 6971–6981. [CrossRef]
11. Menter, F.R. Two-equation eddy-viscosity turbulence models for engineering applications. *AIAA J.* **1994**, *32*, 1598–1605. [CrossRef]
12. Modest, M.F. *Radiative Heat Transfer*, 3rd ed.; Academic Press: Amsterdam, The Netherlands, 2013.
13. Duffie, J.A.; Beckman, W.A. *Solar Engineering of Thermal Processes*, 4th ed.; John Wiley & Sons: Hoboken, NJ, USA, 2013. [CrossRef]

Disclaimer/Publisher's Note: The statements, opinions and data contained in all publications are solely those of the individual author(s) and contributor(s) and not of MDPI and/or the editor(s). MDPI and/or the editor(s) disclaim responsibility for any injury to people or property resulting from any ideas, methods, instructions or products referred to in the content.